VIP **Electrochemistry** *Very Important Paper*

Strong Lithium Polysulfide Chemisorption on Electroactive Sites of Nitrogen-Doped Carbon Composites For High-Performance Lithium–Sulfur Battery Cathodes**

Jiangxuan Song, Mikhail L. Gordin, Terrence Xu, Shuru Chen, Zhaoxin Yu, Hiesang Sohn, Jun Lu, Yang Ren, Yuhua Duan, and Donghai Wang*

Abstract: Despite the high theoretical capacity of lithium–sulfur batteries, their practical applications are severely hindered by a fast capacity decay, stemming from the dissolution and diffusion of lithium polysulfides in the electrolyte. A novel functional carbon composite (carbon-nanotube-interpenetrated mesoporous nitrogen-doped carbon spheres, MNCS/CNT), which can strongly adsorb lithium polysulfides, is now reported to act as a sulfur host. The nitrogen functional groups of this composite enable the effective trapping of lithium polysulfides on electroactive sites within the cathode, leading to a much improved electrochemical performance (1200 mAh g^{-1} after 200 cycles). The enhancement in adsorption can be attributed to the chemical bonding of lithium ions by nitrogen functional groups in the MNCS/CNT framework. Furthermore, the micrometer-sized spherical structure of the material yields a high areal capacity (ca. 6 mAh cm^{-2}) with a high sulfur loading of approximately 5 mg cm^{-2}, which is ideal for practical applications of the lithium–sulfur batteries.

Lithium–sulfur batteries have attracted great interest owing to their high theoretical capacity of 1672 mAh g^{-1} and low costs.[1] Unlike batteries with intercalation compounds, Li–S batteries experience dissolution and diffusion of reaction intermediates (lithium polysulfides, Li$_2$S$_x$, $2 < x \leq 8$) into the electrolyte. This behavior can lead to a loss of active material from the cathode and to a polysulfide shuttle phenomenon, resulting in capacity fading and poor coulombic efficiency.

Many strategies have been developed to address the above-mentioned problems, including the design of novel cathode materials,[2] electrolytes,[3] anode protections,[4] and battery structures.[5] Porous carbon hosts are especially promising, as they can not only improve sulfur utilization by keeping sulfur particles nanometer-sized and electrically connected, but they can also adsorb sulfur and/or polysulfides on their large internal surfaces, rendering redeposition more uniform and mitigating polysulfide diffusion. However, these designs are limited by the weak interactions between the carbon scaffolds and the sulfur species, which are just based on physical adsorption. Consequently, the achieved cyclability is unsatisfactory. Although some other adsorbent additives[6] have also been tested, these are generally non-conductive, requiring the desorption and diffusion of polysulfides before they can be utilized. To date, the capacity of porous carbon–sulfur cathodes is usually limited to 1000 mAh per gram of sulfur, and the electrochemical performance with a high electrode mass loading (> 4 mg of sulfur per cm^2) is rarely evaluated when using the industry-adopted coating techniques.[2a–f]

Recently, we demonstrated that nitrogen doping promotes the chemical bonding between sulfur and oxygen functional groups on carbon.[7] This facilitates the uniform initial distribution and redeposition of sulfur in the carbon host and thus improves the cycling performance. However, this bonding only occurs at a high temperature (e.g., 155°C) upon sulfur loading, and polysulfide diffusion remains a key issue.

Herein, we report the much enhanced adsorption of lithium polysulfides on nitrogen-doped carbon. The functional groups of N-doped carbon are directly utilized to adsorb soluble Li$_2$S$_x$ in the absence of a thermal treatment of the sulfur and doped carbon material; this material shows unprecedentedly strong adsorption abilities and can thus

[*] Dr. J. X. Song, M. L. Gordin, Dr. T. Xu, S. R. Chen, Z. X. Yu,
Dr. H. Sohn, Prof. D. H. Wang
Department of Mechanical and Nuclear Engineering
The Pennsylvania State University
University Park, PA 16802 (USA)
E-mail: dwang@psu.edu

Dr. J. Lu
Chemical Sciences and Engineering Division
Argonne National Laboratory
Argonne, IL 60439 (USA)

Dr. Y. Ren
X-ray Science Division, Argonne National Laboratory
Argonne, IL 60439 (USA)

Dr. Y. H. Duan
National Energy Technology Laboratory
United States Department of Energy
Pittsburgh, PA 15236 (USA)

efficiently trap lithium polysulfides within the cathodes. It was applied in Li–S batteries by synthesizing carbon-nanotube-interpenetrated mesoporous N-doped carbon spheres (MNCS/CNT) with a large porosity and a high material tap density, which was used to fabricate both a cathode with a high sulfur loading and an effective cathode-protecting interlayer. Such cells retained a high capacity of approximately 1200 mAh g^{-1} after 200 deep cycles. This can serve as the basis for significant further work, pushing Li–S batteries closer to practical applications.

The MNCS/CNT composite was synthesized by the facile two-step approach illustrated in Figure 1 a. This strategy relies on evaporation-induced self-assembly (EISA),[8] which can control pore formation through a solvent evaporation process of an oligomer resin precursor [poly(melamine-*co*-formaldehyde), MF] and porogens, such as surfactants (Pluronic F127), SiO$_2$ nanoparticles, and silicate sols, combined with emulsion polymerization, which can control the external morphology of the particles (for experimental details, see the Supporting Information).

Scanning electron microscopy (SEM) images of the composite, which has a micrometer-sized spherical morphology with CNTs protruding to the surface, are shown in Figure 1 b–d. Furthermore, as shown in the Supporting Information, Figure S1, the CNTs are dispersed throughout the particle interior, improving the conductivity of the composite (Figure S2). The average particle diameter as measured by dynamic light scattering is approximately 24 μm (Figure 1 e), which is consistent with the size determined by SEM imaging. The Brunauer–Emmett–Teller specific surface area and the Barrett–Joyner–Halenda pore volume calculated from the N$_2$ sorption isotherms (Figure 1 f) are 615.02 m^{2}g^{-1} and 2.07 cm^{3}g^{-1}, respectively, and the pore size distribution is centered around 28 nm (Figure 1 f, inset).

The surface and bulk chemical compositions of MNCS/CNT were investigated by X-ray photoelectron spectroscopy (XPS) and elemental analysis. XPS spectra of the MNCS/CNT composite show the presence of C, N, and O (Figure 1 g). The binding energy peaks observed in the high-resolution N 1s profile at 398.3 eV and 401.1 eV (Figure 1 g, inset) can be
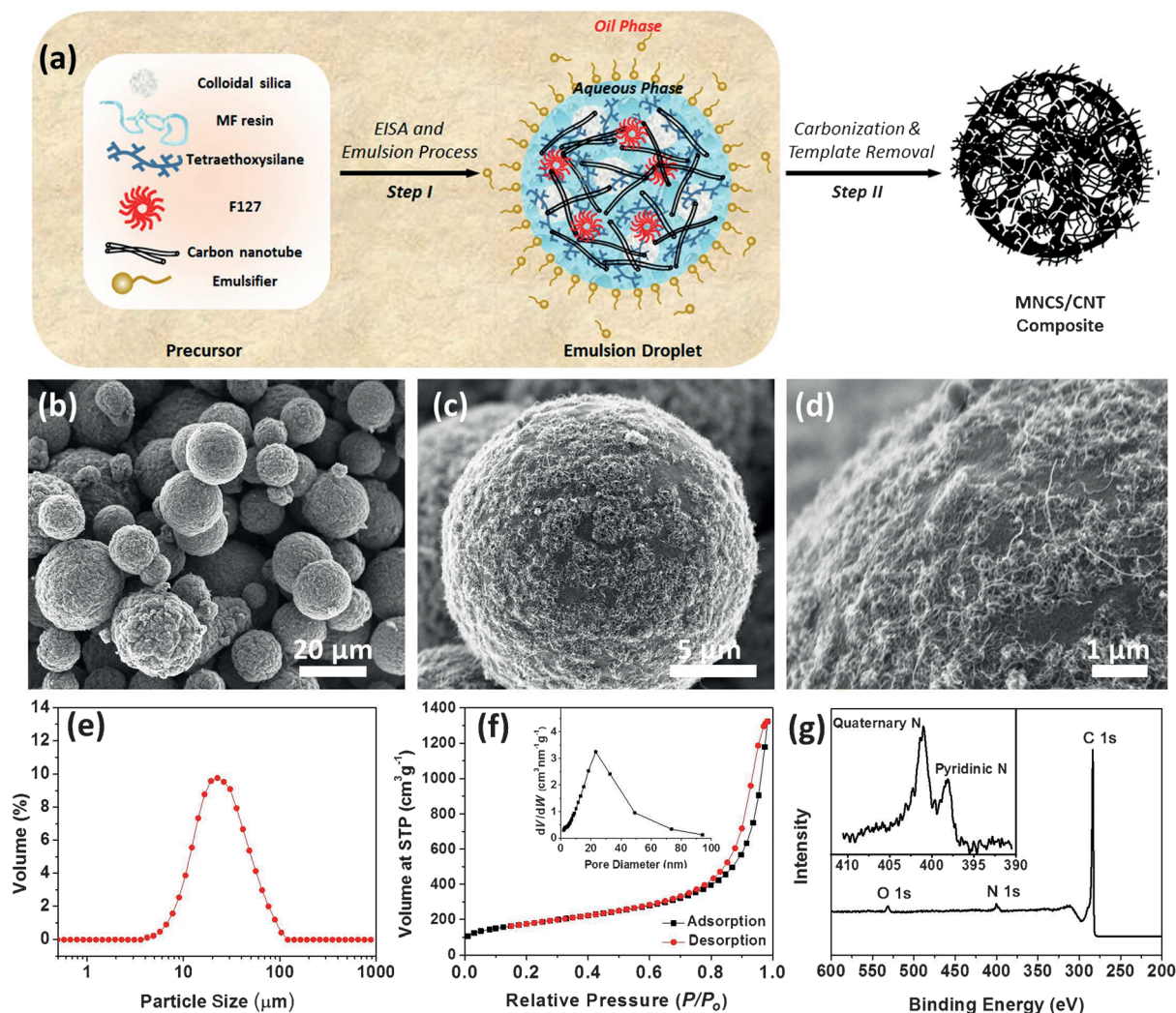

Figure 1. a) Synthesis of the MNCS/CNT composite. b–d) SEM images of the MNCS/CNT composite with low (b), medium (c), or high (d) magnification. e) Size distribution of the MNCS/CNT composite as determined by DLS measurements. f) N$_2$ adsorption and desorption isotherms. Inset: pore size distribution of the MNCS/CNT composite. g) XPS survey spectrum of the MNCS/CNT composite. Inset: high-resolution spectrum of the N 1s peak.

attributed to pyridinic and quaternary nitrogen atoms, respectively.[9] The overall composition of the MNCS/CNT material determined by elemental analysis includes 4.85 wt% nitrogen and 3.73 wt% oxygen (Table S1).

The ability of the MNCS/CNT composite to adsorb Li_2S_x was evaluated by UV/Vis spectroscopy and compared with those of other reported adsorbents. The adsorption amounts (in grams of Li_2S_x per gram of adsorbent; for the calculation, see the Supporting Information) together with the surface areas and pore volumes of these adsorbents are presented in Table S2. Relative adsorption values normalized to the adsorption amount of Super P (carbon black) are shown in Figure 2. The relative adsorption values of the MNCS and MNCS/CNT materials are much higher than those of all other adsorbents. MNCS can adsorb roughly five times as much Li_2S_x as Al_2O_3 nanoparticles and mesoporous carbon (MPC), and an order of magnitude more polysulfide than Super P and SBA-15, although SBA-15 and MPC both have a larger surface area and a greater pore volume than MNCS (Table S2). The color of the Li_2S_x solution also becomes much lighter after exposure to MNCS, further indicating significant adsorption of Li_2S_x (Figure 2, inset).

As discussed earlier, porous carbon hosts cannot only improve the electrical conductivity of the cathode, but also mitigate the diffusion of Li_2S_x. However, Li_2S_x trapping relies on the physical adsorption of Li_2S_x on carbon and consequently has only a weak effect on polysulfide diffusion. Some nonconductive adsorbents, such as oxides[6a,c] or polymers,[2a, 10] have a better ability to trap Li_2S_x; however, their use may lead to ohmic polarization. Furthermore, the adsorbed active materials cannot receive electrons from these non-conductive absorbents, thus preventing electrochemical redox processes. The active materials must desorb and travel to the surface of the conductive host, slowing down the reaction rates and potentially leading to the permanent loss of active material if it becomes too strongly adsorbed. In contrast, the highly conductive N-doped carbon material enables direct and easy redox reactions of adsorbed polysulfides while showing even stronger adsorption.

To investigate the mechanism behind the strong adsorption behavior of N-doped carbon, pair distribution function (PDF) analysis was performed. The PDF profiles for MNCS and MNCS treated with Li_2S_x (MCNS–Li_2S_x) are shown in Figure 2b. For MNCS, interatomic distance peaks of carbon appear at 1.41, 2.46, 3.08, 3.74, 4.32, and 4.94 Å, approximately corresponding to the structure of graphitic carbon ($P6_3mc$). However, in comparison to pristine and ball-milled graphite ($P6_3mc$),[11] the PDFs of both samples show significant peak broadening. In particular, the very broad first peak at 1.41 Å and the shift of the graphite peak at 2.85 Å to 3.08 Å in MNCS indicate the existence of a variety of bonds because of the N and O functional groups in the carbon-based material. An extra interatomic distance peak appears at 1.96 Å in the MCNS–Li_2S_x sample, which may stem from S−S, Li−O, and/or Li−N bonding.[12] Furthermore, a shift of the peak at 3.08 Å to 2.98 Å was noted in the MCNS–Li_2S_x sample, and the first several peaks became narrower. This is indicative of changes in the carbon structure, likely owing to changes in the functional group bonding caused by the adsorption of polysulfides on the N and O functional groups.

We also performed DFT calculations to better understand the possible mechanism of the enhanced adsorption of Li_2S_x on N-doped carbon. The optimized geometries of lithium ions adsorbed on N-free and N-doped model carbon materials are shown in Figure S4. In all cases, it was found that N-doped carbon had more negative Li^+ adsorption energies than undoped carbon (Table 1). This result is in agreement with our experimental results in that N doping can enhance the adsorption of Li^+. This is corroborated by the calculated Mulliken charges (Table S3 a,b), which show that Li^+ has a more negative charge when adsorbed on N, and that N has a more positive charge than C. For N atoms adjacent to oxygen functional groups, the N atoms can transfer their extra electron to the −C=O or −COOH groups, leading to a more negative charge on the oxygen functional group and a more positive charge on the Li^+ ion, thus enabling stronger ionic bonding with Li^+ (Table S3 c–f). These computations clarify how this material is able to enhance lithium polysulfide adsorption and demonstrate one general means of doing so—doping electron-rich atoms into the carbon framework.

To bridge the gap between adsorption behavior and real battery performance, we directly used the MNCS/CNT composite as a sulfur host for Li–S batteries and additionally fabricated a cathode-protecting MNCS/CNT interlayer. The
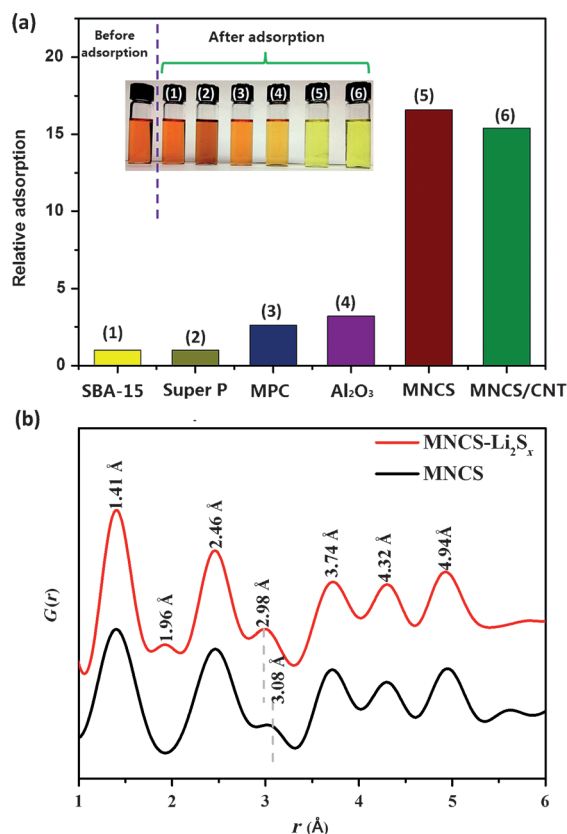

Figure 2. a) Comparison of the relative adsorption amounts for various adsorbents: SBA-15 mesoporous silica, Al_2O_3 nanoparticles, carbon black (Super P), mesoporous carbon (MPC), and nitrogen-doped mesoporous carbon (MNCS and MNCS/CNT). Inset: Photographs of a polysulfide solution before and after exposure to the different adsorbents. b) PDF profiles of MNCS and MNCS–Li_2S_x.

Table 1: Adsorption energies for Li$^+$ on different active sites of nitrogen-free carbon and nitrogen-doped carbon materials as determined by DFT calculations.

| | Nitrogen-free carbon material | | | Nitrogen-doped carbon material | | | | |
	–	–C=O	–COOH	–		–C=O		–COOH
adsorption site	C	O	O	N	N	O	N	O
ΔE [kcal mol^{-1}]	−47.79	−3.74	−69.74	−70.64	−19.35	−57.56	−209.94	−221.01

high surface area and pore volume in MNCS/CNT can accommodate over 70 wt % of sulfur within the carbon matrix to obtain a MNCS/CNT–S composite. This sulfur content was confirmed by thermogravimetric analysis (Figure S5). The uniform distribution of sulfur within the pores of the MNCS/CNT composite was demonstrated by X-ray diffraction, TEM, and electron energy loss spectroscopy (EELS) elemental mapping (Figure S6, S7).

Electrodes were fabricated to test the electrochemical performance of the MNCS/CNT–S composite with an MNCS/CNT interlayer (for experimental details, see the Supporting Information). The high tap density (0.95 g cm^{-3}) and the large particle size of the MNCS/CNT–S composite allow for fairly compact electrodes with a high mass loading of more than 5 mg S cm^{-2} to be made, which is a key factor for reaching high gravimetric/volumetric energy densities in the cell. The sulfur loading in our materials is approximately 2–10 times higher than in most other nanostructured carbon–sulfur electrodes (0.5–2.5 mg cm^{-2}).[2e, 13]

A typical discharge–charge profile of an MNCS/CNT–S cell at a current density of 1.68 mA cm^{-2} between 1.7 and 3.0 V is shown in Figure 3a. No major polarization was observed despite the high sulfur content and the high mass loading. Figure 3b shows the cycling performance of an MNCS/CNT–S cell. A high initial capacity of 1438.3 mAh g^{-1} was attained at 0.84 mA cm^{-2}, corresponding to a sulfur utilization of 86.0 % even with the high sulfur loading. The MNCS/CNT–S cathode showed excellent cycling stability in the following 200 cycles at a higher current of 1.68 mA cm^{-2}, retaining a specific capacity of approximately 1200 mAh g^{-1}. Combined with the material's high tap density, this gives a high volumetric capacity of 1140 mAh cm^{-3} and should help enable a high volumetric capacity in the cell. The efficiency was also quite high, namely around 97.0–99.5 %, owing to both the LiNO$_3$ electrolyte additive and the chemical adsorption of polysulfides induced by nitrogen doping; LiNO$_3$ is known to promote the formation of a stable protective film on the lithium anode.[14] To the best of our knowledge, this is the first report of such high sulfur utilization, excellent cycle stability, and high coulombic efficiency at a high sulfur loading and a high current. To further demonstrate the importance of the adsorption of Li$_2$S$_x$ enabled by nitrogen doping, we studied the performance of cells with simple ball-milled carbon–sulfur cathodes using both the MNCS/CNT interlayer and a previously reported undoped microporous carbon interlayer.[5] As shown in Figure S8, the stability is dramatically better with the MNCS/CNT interlayer than with the undoped interlayer, again supporting the critical role of the strong adsorption in polysulfide trapping.
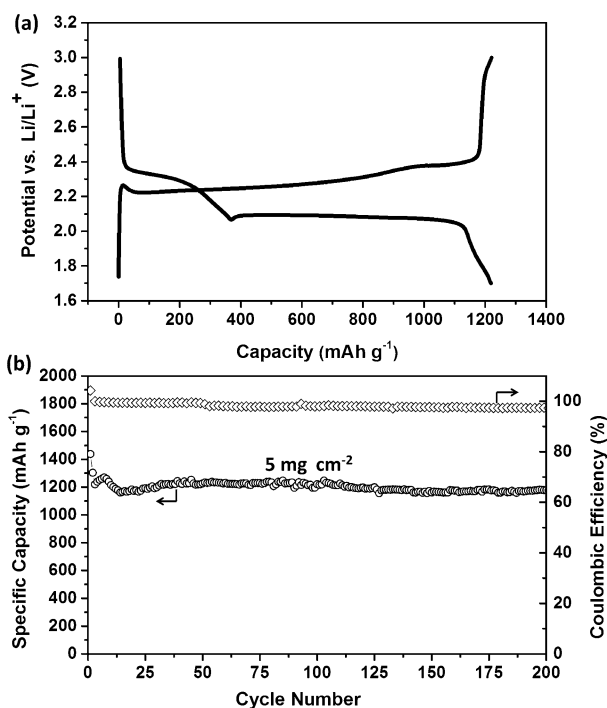

Figure 3. a) A typical discharge–charge voltage–capacity profile of an MNCS/CNT–S cathode. b) Cycling performance of MNCS/CNT–S at a current density of 0.84 mA cm^{-2} for the first cycles and 1.68 mA cm^{-2} for the subsequent cycles. ◇: coulombic efficiency, ○: specific capacity.

When considering practical applications, achieving a high areal capacity is critical, as it increases the ratio of active to inactive materials in the cell. The areal capacity of the electrode is based on the specific capacity and the sulfur mass loading of the electrode. A high sulfur loading is thus necessary for reaching a high areal capacity. In this work, the MNCS/CNT–S composite can deliver an areal capacity of approximately 6 mAh cm^{-2}, which is significantly higher than most areal capacities reported to date (see Figure S9).

The excellent electrochemical performance of the Li–S cells reported here is believed to be due to the unique characteristics of the functional carbon scaffold: First, unlike traditional carbon scaffolds and non-conductive adsorbents, N-doped carbon utilizes chemical adsorption, allowing it to strongly adsorb Li$_2$S$_x$. The MNCS/CNT composite can thus effectively trap soluble polysulfides during cycling, mitigating the loss of active material. Second, unlike reported non-conductive adsorbents, the highly conductive N-doped carbon enables direct and easy redox reactions of adsorbed polysulfides, leading to good electrode kinetics. These factors make the highly conductive, strongly adsorbing N-doped

carbon material an excellent choice for a Li–S battery cathode framework.

In summary, CNT-interpenetrated mesoporous nitrogen-doped carbon spheres have been synthesized through a facile EISA emulsion strategy. The MNCS/CNT composite was used as a sulfur host for Li–S batteries, where it showed an exceptional ability for the adsorption of soluble lithium polysulfides. This adsorption still takes place on a conductive carbon surface, enabling fast and easy redox reactions. The adsorption mechanism was found to be related to the electron-donating ability of the doped N atoms. In this way, the MNCS/CNT composite can significantly inhibit the dissolution of polysulfides and retard the loss of active material, and as a result, it can deliver a high initial specific capacity (1480 mAh g^{-1}) and excellent cycling stability (90% retention over 200 cycles after activation) at a high sulfur content of 70 wt% and a high sulfur loading of approximately 5 mg cm^{-2}. These numerous advantages make the MNCS/CNT composite a promising material for practical applications. Furthermore, these results illustrate a general means of enhancing the performance of carbon scaffolds for Li–S batteries, the doping of electron-rich elements, which can be used to further enhance the properties of other materials and drive future research on Li–S battery cathodes.

[1] a) A. Manthiram, Y. Fu, S.-H. Chung, C. Zu, Y.-S. Su, *Chem. Rev.* **2014**, *114*, 11751–11787; b) Y. Yang, G. Zheng, Y. Cui, *Chem. Soc. Rev.* **2013**, *42*, 3018–3032.

[2] a) X. Ji, K. T. Lee, L. F. Nazar, *Nat. Mater.* **2009**, *8*, 500–506; b) N. Jayaprakash, J. Shen, S. S. Moganty, A. Corona, L. A. Archer, *Angew. Chem. Int. Ed.* **2011**, *50*, 5904–5908; *Angew. Chem.* **2011**, *123*, 6026–6030; c) L. Ji, M. Rao, H. Zheng, L. Zhang, Y. Li, W. Duan, J. Guo, E. J. Cairns, Y. Zhang, *J. Am. Chem. Soc.* **2011**, *133*, 18522–18525; d) Z. Wei Seh, W. Li, J. J. Cha, G. Zheng, Y. Yang, M. T. McDowell, P.-C. Hsu, Y. Cui, *Nat. Commun.* **2013**, *4*, 1331; e) S. Xin, L. Gu, N.-H. Zhao, Y.-X. Yin, L.-J. Zhou, Y.-G. Guo, L.-J. Wan, *J. Am. Chem. Soc.* **2012**, *134*, 18510–18513; f) L. Xiao, Y. Cao, J. Xiao, B. Schwenzer, M. H. Engelhard, L. V. Saraf, Z. Nie, G. J. Exarhos, J. Liu, *Adv. Mater.* **2012**, *24*, 1176–1181; g) C. Tang, Q. Zhang, M.-Q. Zhao, J.-Q. Huang, X.-B. Cheng, G.-L. Tian, H.-J. Peng, F. Wei, *Adv. Mater.* **2014**, *26*, 6100–6105.

[3] a) Z. Lin, Z. Liu, W. Fu, N. J. Dudney, C. Liang, *Angew. Chem. Int. Ed.* **2013**, *52*, 7460–7463; *Angew. Chem.* **2013**, *125*, 7608–7611; b) M. L. Gordin, F. Dai, S. Chen, T. Xu, J. Song, D. Tang, N. Azimi, Z. Zhang, D. Wang, *ACS Appl. Mater. Interfaces* **2014**, *6*, 8006–8010.

[4] C. Huang, J. Xiao, Y. Shao, J. Zheng, W. D. Bennett, D. Lu, L. V. Saraf, M. Engelhard, L. Ji, J. Zhang, X. Li, G. L. Graff, J. Liu, *Nat. Commun.* **2014**, *5*, 3015.

[5] Y.-S. Su, A. Manthiram, *Nat. Commun.* **2012**, *3*, 1166.

[6] a) X. Ji, S. Evers, R. Black, L. F. Nazar, *Nat. Commun.* **2011**, *2*, 325; b) Y. Zhang, L. Wang, A. Zhang, Y. Song, X. Li, H. Feng, X. Wu, P. Du, *Solid State Ionics* **2010**, *181*, 835–838; c) Y. J. Choi, B. S. Jung, D. J. Lee, J. H. Jeong, K. W. Kim, H. J. Ahn, K. K. Cho, H. B. Gu, *Phys. Scr.* **2007**, *T129*, 62–65.

[7] J. Song, T. Xu, M. L. Gordin, P. Zhu, D. Lv, Y.-B. Jiang, Y. Chen, Y. Duan, D. Wang, *Adv. Funct. Mater.* **2014**, *24*, 1243–1250.

[8] R. Liu, Y. Shi, Y. Wan, Y. Meng, F. Zhang, D. Gu, Z. Chen, B. Tu, D. Zhao, *J. Am. Chem. Soc.* **2006**, *128*, 11652–11662.

[9] J. R. Pels, F. Kapteijn, J. A. Moulijn, Q. Zhu, K. M. Thomas, *Carbon* **1995**, *33*, 1641–1653.

[10] Z. W. Seh, Q. Zhang, W. Li, G. Zheng, H. Yao, Y. Cui, *Chem. Sci.* **2013**, *4*, 3673–3677.

[11] P. Valeri, T. Adam, C. John, R. Yang, *J. Phys. Condens. Matter* **2011**, *23*, 435003.

[12] a) E. Kaufmann, S. Sieber, P. v. R. Schleyer, *J. Am. Chem. Soc.* **1989**, *111*, 4005–4008; b) W. Gordy, *J. Chem. Phys.* **1947**, *15*, 305–310.

[13] a) S. Chen, F. Dai, M. L. Gordin, D. Wang, *RSC Adv.* **2013**, *3*, 3540–3543; b) H. Wang, Y. Yang, Y. Liang, J. T. Robinson, Y. Li, A. Jackson, Y. Cui, H. Dai, *Nano Lett.* **2011**, *11*, 2644–2647; c) Y. M. Lee, N.-S. Choi, J. H. Park, J.-K. Park, *J. Power Sources* **2003**, *119–121*, 964–972.

[14] S. S. Zhang, *Electrochim. Acta* **2012**, *70*, 344–348.